

# The structural and photometric properties of early-type galaxies in hierarchical models

C. Almeida<sup>1</sup>, C. M. Baugh<sup>1</sup>, C. G. Lacey.<sup>1</sup>

<sup>1</sup>*Institute for Computational Cosmology, Department of Physics, University of Durham, South Road, Durham, DH1 3LE, UK.*

25 May 2019

## ABSTRACT

We present predictions for the structural and photometric properties of early-type galaxies in the cold dark matter cosmology ( $\Lambda$ CDM). We use the GALFORM code, which tracks the evolution of the disk and bulge components of a galaxy, using a self-consistent model to compute the scalelengths. The sizes of galactic disks are determined by the conservation of the angular momentum of cooling gas. The sizes of merger remnants are computed by applying the virial theorem and conserving the binding energy of the progenitors and their orbital energy. We compare the model predictions with observational results derived from the SDSS. The model enjoys a number of notable successes, such as reproducing the local Faber-Jackson relation (velocity dispersion-luminosity), the velocity dispersion-age relation, and the fundamental plane relating the luminosity, velocity dispersion and effective radius of spheroids. We study how the residuals around the zero-point of the fundamental plane depend on galaxy properties. However, there are some important disagreements between the model predictions and observations: the brightest model spheroids have effective radii smaller than observed and the zero-point of the fundamental plane shows little or no evolution with redshift in the model. We examine in detail the physical ingredients of our calculation of galaxy sizes, showing which components have the most influence on our results.

## 1 INTRODUCTION

Remarkably tight correlations exist between the structural and photometric properties of galaxies. Across the Hubble sequence there is a strong dependence of luminosity on either the rotation speed of galactic disks (Tully & Fisher 1977) or the velocity dispersion of spheroids (Faber & Jackson 1976). Other scaling relations observed for early-type galaxies include those between colour and magnitude (Sandage & Visvanathan 1978a,b), colour and velocity dispersion (Bernardi et al. 2005), radius and luminosity (Sandage & Perelmuter 1990), and radius and surface brightness (Kormendy 1977). Some of these correlations can be combined into a “fundamental plane” which connects the effective radii, velocity dispersions and luminosities of ellipticals (Djorgovski & Davis 1987; Dressler et al. 1987; Bernardi et al. 2003a).

The existence of these scaling relations and their tightness encode clues about the formation and evolution of elliptical galaxies. For example, the existence of the fundamental plane can be understood by applying the virial theorem to a gravitationally bound stellar spheroid in dynamical equilibrium, after making the assumption that ellipticals of different sizes have the same structure (homology) and a constant mass-to-light ratio. The deviation of the observed fundamental plane from this prediction can therefore

be driven by variations in the mass-to-light ratio across the early-type population or by a non-uniformity of the structure of ellipticals, referred to as structural non-homology, or a combination of these two effects (Trujillo et al. 2004). At first sight, the small scatter around the zero-point of the observed correlations would appear to pose a challenge to hierarchical galaxy formation models, since the variety of merger histories in the models would lead one to expect to a corresponding scatter in the properties of early-type galaxies.

In this paper, we use a semi-analytical approach to model the properties of elliptical galaxies. Such models predict the star formation and merger histories of galaxies (for a review of this class of model, see Baugh 2006). In general, two channels are considered for the formation of spheroids: galaxy mergers or secular evolution of the disk. We will describe the formation of disks and bulges in more detail in Section 2. The first attempts to track the disk and bulge of a galaxy separately simply recorded the mass and luminosity in each component (Baugh, Cole & Frenk 1996; Kauffmann 1996). The models have now progressed to a stage where detailed predictions can be produced for the structural properties of galaxies in addition to their stellar populations. Cole et al. (2000) introduced a model for the sizes of the disk and spheroid components of galaxies: the size of a galactic disk is calculated by assuming conservation of

arXiv:astro-ph/0608544v1 25 Aug 2006

the angular momentum of the gas as it cools and collapses in the halo; the size of the spheroid is derived by applying conservation of binding and orbital energy, and by applying the virial theorem to the merging galaxies. The Cole et al. scheme also takes into account the gravitational force of the dark matter and the reaction of the dark matter halo to the presence of the baryons (see Section 2 for further details).

Cole et al. tested their model for the sizes of galactic disks against the observed distribution of disk scale lengths estimated by De Jong & Lacey (2000), and verified that the predictions of their fiducial model were in excellent agreement with the observations.

Cole et al. did not test their prescription for predicting the size of galactic spheroids. This is the focus of our paper.

Hatton et al. (2003) used a similar scheme to that outlined by Cole et al. to compute the sizes of spheroids in the GALICS model. However, these authors adopted a less realistic model for the scale size of galactic disks. In common with many semi-analytical models, they assumed that the scale size of a disk is related to the virial radius of the host dark matter halo by  $r_D = \lambda R_{200}/2$ , where  $\lambda$  is the dimensionless spin parameter for the dark matter halo, which quantifies its angular momentum, and  $R_{200}$  is the halo virial radius. This ignores the self-gravity of the baryons and the contraction they produce in the central regions of the dark matter halo. Several papers have considered the origin of the fundamental plane and the role of gas-rich and gas-poor mergers using numerical simulations, which follow the dark matter and baryons (Kobayashi 2005; Dekel & Cox 2006; Robertson et al. 2006; Boylan-Kolchin et al. 2006).

In Section 2, we summarize our model, explaining the ingredients which are particularly pertinent to the formation of galactic spheroids. We first compare our predictions to the sample of early-type galaxies drawn from the Sloan Digital Sky Survey by Bernardi et al. (2005): the selection criteria are described in Section 3 and the comparisons between our model predictions and the data are given in Section 4. The evolution with redshift of the model predictions for the scaling relations is presented in Section 5. In Section 6, we explore the sensitivity of our model predictions to various physical ingredients of the models. Our conclusions are given in Section 7.

## 2 THE GALAXY FORMATION MODEL

A comprehensive overview of the GALFORM model of galaxy formation and the philosophy behind semi-analytical modelling can be found in Cole et al. (2000). Important extensions to the model are described in Benson et al. (2002) and Benson et al. (2003). In this paper, we focus on the predictions of the model introduced by Baugh et al. (2005). These authors put forward the first fully consistent hierarchical galaxy formation model which was able to explain the observed number counts of sub-mm sources and the luminosity function of Lyman-break galaxies, at the same time as reproducing the observed properties of the low redshift galaxy population. We also show predictions from the model described by Bower et al. (2006), which includes feedback processes associated with the accretion of material onto a supermassive black hole, using the model of black hole growth explained in Malbon et al. (2006). Baugh et al. assumed a

flat  $\Lambda$ CDM cosmology, with  $\Omega_0 = 0.3$ ,  $\Omega_\Lambda = 0.7$ ,  $\Omega_b = 0.04$ ,  $h = H_0/(100 \text{ km s}^{-1}\text{Mpc}^{-1}) = 0.7$ , and  $\sigma_8 = 0.93$ . In the Bower et al. model, the cosmological parameters have slightly different values to match those used in the Millennium Simulation:  $\Omega_0 = 0.25$ ,  $\Omega_\Lambda = 0.75$ ,  $\Omega_b = 0.045$ ,  $h = 0.73$ , and  $\sigma_8 = 0.9$  (Springel et al. 2005). Selected predictions from the Bower et al. model can be downloaded over the internet (see Lemson et al. 2006).

We now give a brief overview of the GALFORM model, referring the reader to the references given in the previous paragraph for further details. We then recap some of the ingredients of the model which are particularly important for determining the masses and sizes of galactic spheroids and disks.

The aim of the GALFORM model is to make an *ab initio* calculation of the formation and evolution of the galaxy population, set in the context of a cosmological model in which structures in the dark matter form hierarchically through gravitational instability. The main physical processes which we attempt to incorporate into the model are the following: (i) The hierarchical merging and collapse of dark matter haloes. (ii) The radiative cooling of shock heated gas. (iii) Quiescent star formation in discs. (iv) Feedback processes driven by supernovae and by the accretion of material onto supermassive black holes in the case of the model of Bower et al. (2006). (v) The effect of a photoionizing background of radiation on the intergalactic medium and on galaxy formation (see Benson et al. 2002). (vi) The chemical enrichment of the gas and stars. (vii) The decay of the orbits of galactic satellites due to dynamical friction. This can lead to mergers between galaxies which can trigger bursts of star formation and a change in galaxy morphology (see the next subsection).

The model generates a star formation history and a galaxy merger history for a representative population of galaxies at any epoch. Each galaxy is split into two components, a disk and a bulge. The formation of these components is discussed in the next subsection.

There are a number of differences between the Baugh et al. (2005) and Bower et al. (2006) models. In the Baugh et al. model, the formation of massive galaxies is suppressed by a superwind (see Benson et al. 2003). The mass ejected by the wind is a multiple of the star formation rate. There is evidence of such outflows in the spectra of Lyman-break galaxies and in local starburst galaxies (Adelberger et al. 2003; Wilman et al. 2005). In the Bower et al. model, the cooling of gas is suppressed in massive haloes due to the heating of the halo gas by energy released by the accretion of matter onto a central supermassive black hole. There is also less star formation in bursts in the Bower et al. model, due to the way in which the timescale for quiescent star formation in disks scales with the local dynamical time (this timescale is independent of redshift in the Baugh et al. model) and because minor mergers do not trigger starbursts. Baugh et al. assumed that stars are produced with a flat initial mass function (IMF) in bursts. This assumption was primarily responsible for the success of the Baugh et al. model in reproducing the number counts of sub-millimetre detected galaxies. Nagashima et al. (2005a,b) demonstrate that the assumption of a flat IMF is also needed to match the abundance of elements in the hot gas in clusters and the chemical abundances observed in elliptical galaxies.

### 2.1 The formation of spheroids and disks

We assume that gas initially settles into a rotationally supported disk when it cools from the hot halo. This gas eventually turns into stars in the quiescent star formation mode. The effective timescale on which the star formation takes place does not depend upon the dynamical time of the disk in the model of Baugh et al. (2005), but does have some dependence on the circular velocity of the disk.

The formation of galactic spheroids takes place through two channels: galaxy mergers and the instability of galactic disks. Baugh et al. only consider the galaxy merger mode of spheroid formation; Bower et al. consider both mechanisms.

The consequences of a galaxy merger are characterized by the ratio,  $R = m_{\text{sat}}/m_{\text{central}}$ , of the mass of the accreted satellite galaxy ( $m_{\text{sat}}$ ) to the mass of the primary or central galaxy in the halo ( $m_{\text{central}}$ ), onto which the satellite is accreted. The mass ratio  $R$  is compared to two thresholds,  $f_{\text{ellip}}$  and  $f_{\text{burst}}$ , to establish the severity of the merger (see, for example, Bournaud et al. 2005). These thresholds are model parameters. If  $R > f_{\text{ellip}} = 0.3$ , then the galaxy merger is termed ‘‘major’’. In the case of major mergers, the disk of the primary galaxy is destroyed. All stars are transferred to the spheroid component and any cold gas present participates in a burst of star formation which adds stars to the spheroid. If the mass ratio of satellite to primary falls between the thresholds, i.e.  $f_{\text{burst}} < R < f_{\text{ellip}}$ , then the stellar disk of the primary survives and the stars from the accreted satellite are added to the spheroid. In this case, if the primary is also gas rich, that is if cold gas accounts for at least 75% of the total mass in the disk, then we assume that the accretion of the satellite induces an instability which drains the primary disk of cold gas, leading to a burst of star formation in the spheroid.

In our model, a galaxy can move in either direction along the Hubble sequence (Baugh et al. 1996). The accretion of gas from the hot halo and subsequent quiescent star formation leads to a late-type (disk dominated) galaxy. A major merger between two such galaxies produces a descendent galaxy which jumps to the opposite end of the Hubble sequence, becoming an early-type galaxy (bulge dominated). Further accretion of cooling gas allows the galaxy to grow a new disk around its bulge, moving the galaxy back towards the late-type part of the sequence.

In addition to the merger mode of spheroid production, Bower et al. also consider the secular production of bulges from disks which are unstable due to their strong self-gravity. This mode is most important in less massive galaxies.

### 2.2 The scale lengths of the disk and bulge components of galaxies

We assume that disks have an exponential profile, with a half-mass radius given by  $r_{\text{disk}}$ , and bulges have a  $r^{1/4}$  profile in projection, with a half mass in 3D given by  $r_{\text{bulge}}$ .

The scalelength of the disk is determined by the angular momentum of the halo gas, which arises due to the tidal torques which act during the formation of the halo. The angular momentum of the halo gas is quantified by the dimensionless spin parameter,  $\lambda$ ; this quantity is assumed to follow a log-normal distribution matching the re-

sults of N-body simulations (see Cole et al. 2000, for details). We assume that the angular momentum of the gas is conserved as it cools to form a rotationally supported disc (see Okamoto et al. 2005, for a discussion of this assumption).

Spheroids are formed in galaxy mergers or through disk instabilities as outlined in the previous subsection. The size of the spheroid resulting from a galaxy merger,  $r_{\text{m}}$ , is determined by applying the conservation of energy and the virial theorem (see Section 4.4.2 of Cole et al. 2000):

$$\frac{(M_1 + M_2)^2}{r_{\text{m}}} = \frac{M_1^2}{r_1} + \frac{M_2^2}{r_2} + \frac{f_{\text{orbit}}}{c} \frac{M_1 M_2}{r_1 + r_2}, \quad (1)$$

where  $M_i$  represents the total mass (stellar, cold gas and dark matter) of one of the merging objects, within  $r_i$ , and the form factor  $c$  and the parameter  $f_{\text{orbit}}$  are related to the self-binding energy and orbital energy by

$$E_{\text{bind}} = -c \frac{GM_i^2}{r_i} \quad (2)$$

$$E_{\text{orbit}} = -\frac{f_{\text{orbit}}}{2} \frac{GM_1 M_2}{r_1 + r_2}. \quad (3)$$

For simplicity, we adopt  $c = 0.5$  and  $f_{\text{orbit}} = 1$ . Later on, we explore the impact on our predictions of varying  $f_{\text{orbit}}$ . Similar arguments are applied to calculate the scale size of the spheroid which results from an unstable disk (see Section 4.4.3 of Cole et al. 2000).

Once the scale lengths of the disk and bulge components have been calculated as outlined above, we next take into account the selfgravity of the baryons and the contraction of the dark matter halo in response to the gravity of the condensed baryons. New radii are computed for the disk and bulge by applying an adiabatic contraction of the disk, bulge and dark matter components (Blumenthal et al. 1986; Jesseit et al. 2002). In the case of the disk, the total specific angular momentum is conserved. The bulge and dark matter halo are not rotationally supported. Nevertheless, it is useful to define an equivalent circular velocity using the velocity dispersion of each of these components, and, using this, to define a quantity which we refer to as a pseudo-angular momentum. For the bulge the pseudo-angular momentum is given by:  $r_{\text{bulge}} V_c(r_{\text{bulge}})$ . This quantity is conserved during the adiabatic contraction. A similar quantity is conserved for the dark matter.

## 3 THE SELECTION OF AN EARLY-TYPE SAMPLE

We first compare our model predictions against the scaling relations and statistics of the sample of early-type galaxies constructed from the SDSS by Bernardi et al. (2003a, 2005). These authors measured relations between luminosity and various properties of early-type galaxies such as velocity dispersion, effective radius, effective mass, effective density and surface brightness (Bernardi et al. 2003b, 2005). The sample was also used to measure the luminosity function of early-type galaxies (Bernardi et al. 2003b), the fundamental plane (Bernardi et al. 2003c) and the colour-magnitude/colour-velocity dispersion relations (Bernardi et al. 2003d, 2005).

For a complete description of the construction of the early-type sample from the SDSS, we refer the reader to

the above papers. Below we give a summary of the selection criteria applied by Bernardi et al. (2005) (hereafter Ber05). Galaxies are included in the sample if they have:

- (i) Redshift  $z \leq 0.3$ , with a median  $z_{\text{med}} = 0.13$ .
- (ii) Apparent  $r$ -band Petrosian magnitudes in the range  $14.5 < r_{\text{petro}} < 17.75$ .
- (iii)  $\text{eclass} < 0$ . The  $\text{eclass}$  value is a classification of the spectral type of a galaxy derived from a principal component decomposition of its spectrum (Connolly & Szalay 1999). Ber05 chose negative values of  $\text{eclass}$  as this corresponds to spectra in which absorption lines dominate, characteristic of early-type galaxies.
- (iv)  $\text{fracDev} > 0.8$ , computed using the  $r$ -band image. The value of  $\text{fracDev}$  is an indicator of morphology. It is calculated in two steps, in turn. First, the best fit de Vaucouleurs and exponential profiles to the galaxy image are found. Second, using the scale lengths of the best fit profiles found in step one, the best fit linear combination of the disk and bulge profiles is derived. The contribution of the de Vaucouleurs profile to this linear combination is the value of  $\text{fracDev}$ .

We attempt to reproduce these selection criteria by imposing the following conditions on **GALFORM** galaxies:

- (i) We generate a population of galaxies at an output redshift of  $z = 0.13$ , the median redshift of the Ber05 sample. In our comparisons, we consider only Ber05 galaxies that lie within the redshift interval  $0.11 < z \leq 0.15$ , close to the median redshift. This additional selection in redshift reduces the size of the observational sample by a factor of  $\sim 4$  to  $\sim 11000$  objects.

- (ii) We use total magnitudes to select a sample of model galaxies. We apply the same apparent magnitude limits which are used for the data. This is a reasonable approach as the difference between total and Petrosian magnitudes is typically smaller than 0.2 mag (Graham et al. 2005). We have also computed Petrosian magnitudes for our model galaxies and find that using the Petrosian magnitudes in place of total magnitudes does not make a significant difference to our results.

- (iii) At present, **GALFORM** does not produce spectra with absorption line features. Therefore we cannot directly calculate a value for the spectral parameter  $\text{eclass}$ . Instead, we use the  $g - r$  colour which is more readily predicted for model galaxies. In Fig. 1, we use the SDSS DR4 to show that there is a good correlation between  $g - r$  colour and  $\text{eclass}$ . We retain galaxies with  $g - r \gtrsim 0.8$ ; Fig. 1 shows that more than 95% of the galaxies with a negative value for  $\text{eclass}$  are selected by this colour cut.

- (iv) We compute the value of  $\text{fracdev}$  in the same way as was done for the SDSS galaxies. We adopt a cut on  $\text{fracdev} > 0.8$ . In Section 4.1, we explore the impact on our predictions of replacing the cut in the value of  $\text{fracdev}$  with a simple cut on the bulge-to-total luminosity ratio of the model galaxies.

- (v) Due to limitations of the SDSS data we also set a surface brightness threshold,  $\mu_e < 24.5$  mag arcsec $^{-2}$ .

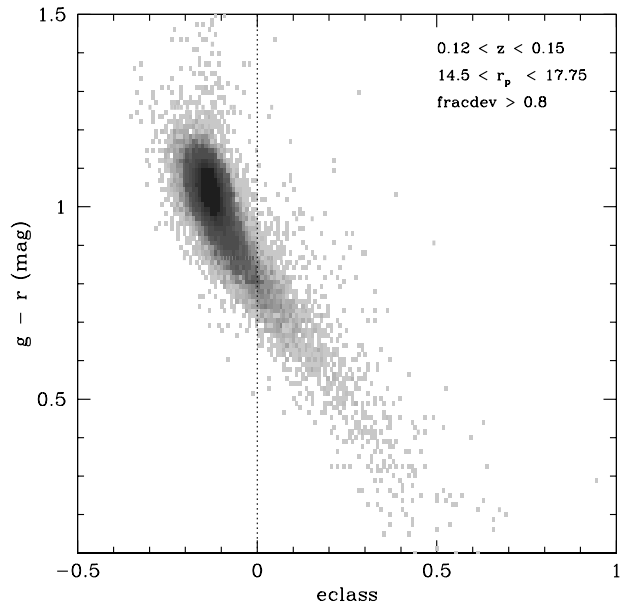


**Figure 1.** The relation between  $g - r$  colour and  $\text{eclass}$ , for a sample of galaxies selected from SDSS DR4 in the redshift range  $0.12 < z < 0.15$  and with Petrosian magnitudes in the interval  $14.5 < r_{\text{petro}} < 17.75$ . The dotted line represents the selection applied to the observational data,  $\text{eclass} < 0$ , by Bernardi et al. (2005): more than 95% of these galaxies have  $g - r > 0.8$ .

## 4 RESULTS

In this section, we compare the predictions of the Baugh et al. (2005) model with observational data for early-type galaxies derived from the SDSS sample of Ber05.

### 4.1 The luminosity function of early-type galaxies

The luminosity function is perhaps the most fundamental statistical description of the galaxy population. Later on, we perform fits to the fundamental plane of early-type galaxies in our model. The results for this fit are sensitive to the abundance of galaxies as a function of luminosity, so it is imperative that the model reproduces the observed luminosity function closely.

In Fig. 2, we compare the predictions of the **GALFORM** model for the  $r$ -band luminosity function of early-type galaxies with the estimate from the SDSS sample of Ber05. The luminosity function of SDSS early-types is well described by a Gaussian form:  $\phi(M) dM = \phi_*/\sqrt{2\pi\sigma^2} \exp\{-(M - M_* + Qz_i)^2/(2\sigma^2)\}$ , where  $(\phi_*, M_*, \sigma, Q) = (1.99 \times 10^{-3} \text{Mpc}^{-3}, -21.15, 0.841, 0.85)$  respectively (note, Ber05 assume  $h = 0.7$ ). The model predictions are in reasonably good agreement with the luminosity function estimated from the data.

We also show, in Fig. 2, the effect of changing the criteria used to select early-type galaxies in the model. In our standard selection, the primary indicator of morphology is  $\text{fracdev}$  (see Section 3). We have also explored using the bulge-to-total luminosity ratio in the  $r$ -band,  $B/T_r$ , in place of  $\text{fracdev}$  (Baugh et al. 1996). The results for cuts of  $B/T_r > 0.8$  and  $B/T_r > 0.5$  are shown by the dotted and

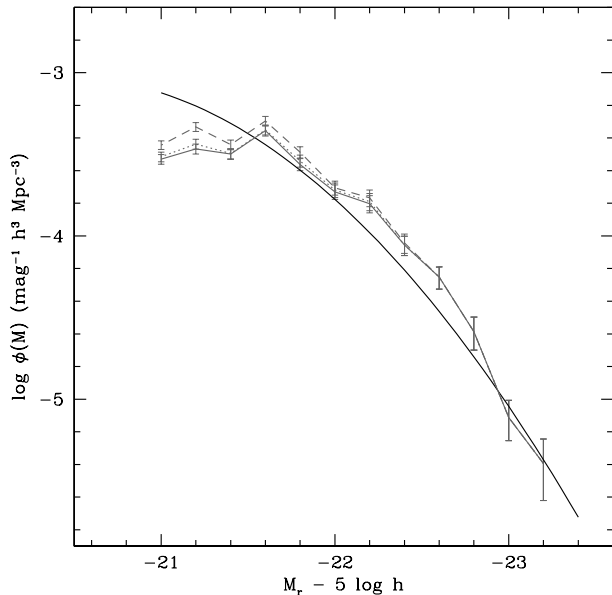


**Figure 2.** The luminosity function of early-type galaxies at  $z = 0.13$ . The solid black line shows a fit to the luminosity function of the SDSS sample of Bernardi et al. (2005). The results for the GALFORM sample are plotted using grey lines. The solid grey line shows our standard early-type galaxy selection, as outlined in Section 3. The errorbars show Poisson errors due to the finite number of galaxies simulated. The other lines show how the luminosity function varies when, instead of using  $\text{fracdev} > 0.8$ , the bulge-to-total  $r$ -band luminosity ratio is used; the dashed line shows the results for  $B/T_r > 0.5$  and the dotted line for  $B/T_r > 0.8$ .

dashed lines respectively in Fig. 2. The luminosity function derived using  $B/T_r > 0.8$  is remarkably similar to the one obtained using  $\text{fracdev} > 0.8$  (shown by the solid grey line).

In our subsequent comparisons with the SDSS sample of early-types, we assign each model galaxy a weight which depends upon luminosity, such that the luminosity function of early-types in the model is forced to reproduce exactly the luminosity function of the data.

#### 4.2 The Faber-Jackson and $\sigma$ -age relations

The Faber-Jackson (hereafter FJ) relation was one of the first scaling relations to be discovered for early-type galaxies (Faber & Jackson 1976). This relation indicates that luminosity is a strong function of velocity dispersion,  $\sigma$ , with brighter early-types displaying larger velocity dispersions. Observational studies suggest that this relation is approximately given by  $L \propto \sigma^4$ : Forbes & Ponman (1999), using a local sample of early-type galaxies, found  $L_B \propto \sigma^{3.9}$  in the B-band, while Pahre et al. (1998) reported  $L_K \propto \sigma^{4.1}$  in the K-band. These results also indicate that the FJ relation is essentially independent of wavelength. In the case of SDSS early-type galaxies, Bernardi et al. (2003b) confirmed these earlier results, finding  $L_r \propto \sigma^{3.91}$  in the  $r$ -band at  $z = 0$ , with no significant differences in slope apparent in the  $g$ ,  $i$  or  $z$ -bands.

Fig. 3 shows the velocity dispersion-magnitude relation

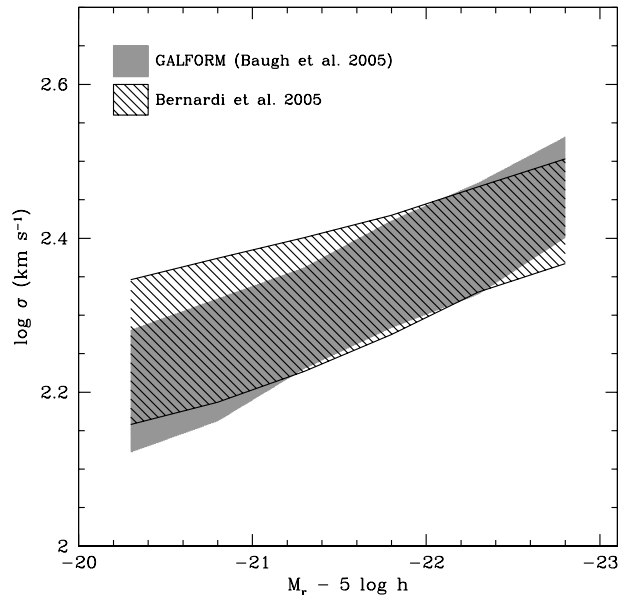


**Figure 3.** The Faber-Jackson relation between luminosity and velocity dispersion. The GALFORM prediction is shown in grey and the hatched shaded region shows the relation for the Ber05 sample. The shaded and hatched regions connect the 10 and 90 percentiles.

predicted by GALFORM. The one-dimensional velocity dispersion is calculated using  $\sigma_{1D} = (1.1/\sqrt{3})V_{c,\text{bulge}}$ , where  $V_{c,\text{bulge}}$  is the effective circular velocity of the bulge, which is assumed to be isotropic (see Cole et al. 1994). The factor of 1.1 is an empirical correction which Cole et al. employed to map data for elliptical galaxies onto the Tully-Fisher relation for spiral galaxies. Fig. 3 shows that retaining this factor gives good agreement with the observed FJ relation. We find no change in the predictions if we consider, instead, the effective circular velocity of the disk and bulge combined. This is a consequence of our selection which ensures that the model galaxies we consider are bulge dominated, as shown by Fig. 2. We find very good agreement between model predictions and the FJ relation observed for the Ber05 sample, albeit with a slightly shallower slope,  $L_r \propto \sigma^{3.2 \pm 0.1}$  (note, we plot  $\sigma$  on the  $y$ -axis). We find little dependence of the slope of the FJ relation on passband, in agreement with observations.

The evolution of the FJ relation with redshift is plotted in Fig. 4. Here, we have chosen output redshifts in GALFORM to match the median redshifts of the Ber05 redshift subsamples: for SDSS galaxies with  $z < 0.08$  we use  $z_{\text{med}} = 0.06$  for the model galaxies, and for SDSS galaxies with  $z > 0.18$  we set  $z_{\text{med}} = 0.20$ . Little evolution is observed in the zeropoint of the FJ relation with redshift, a trend which is reproduced by the model predictions. The shift to brighter magnitudes with increasing redshift is simply a reflection of the fixed apparent magnitude limit of the SDSS. As we shall see in next section, this absence of evolution is actually expected at these redshifts due to the cancellation of two different evolutionary effects.

Finally, in Fig. 5, we plot the luminosity-weighted age of the stellar population, computed in the  $r$ -band, as a function

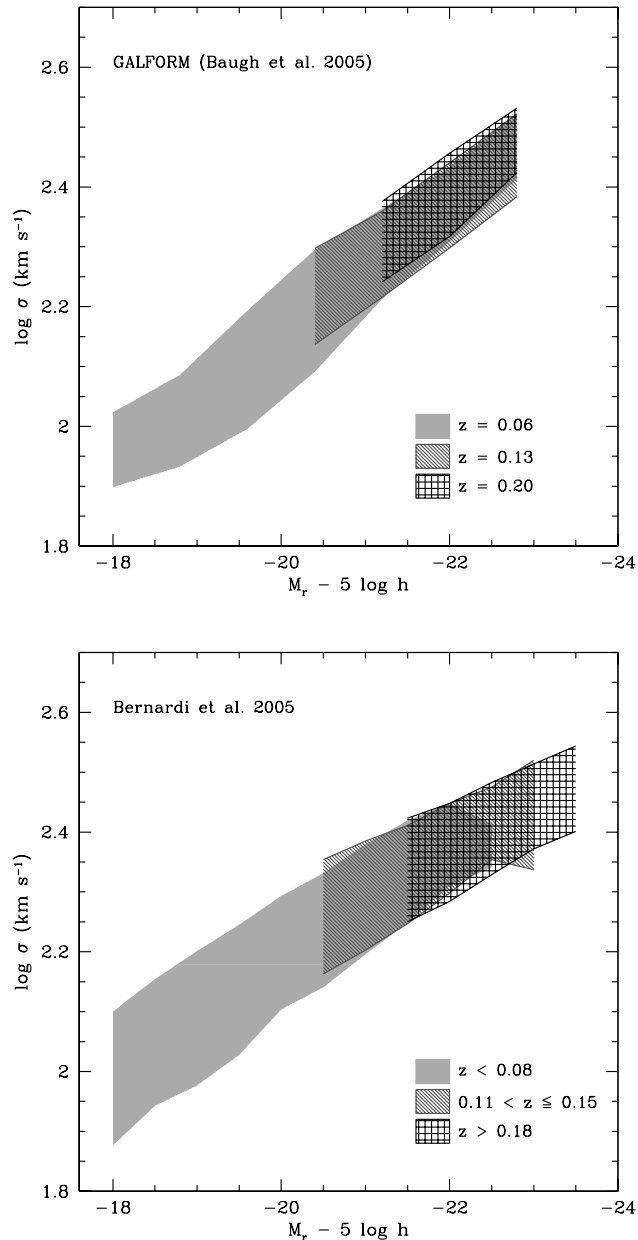


**Figure 4.** The evolution of the Faber-Jackson relation for early-type galaxies. The upper panel shows the model predictions at redshifts  $z = 0.06$ ,  $z = 0.13$  and  $z = 0.20$ , which are the median redshifts of the observational subsamples shown in the lower panel. Shaded regions connect the 10 and 90 percentiles of the distributions.

of the velocity dispersion. Some authors have argued that a correlation exists between these quantities, which has implications for the scatter in the FJ relation (Forbes & Ponman 1999; Nelan et al. 2005). Fig. 5 reveals that velocity dispersion and luminosity-weighted age are indeed correlated in the model, with galaxies which have larger velocity dispersions also displaying older stellar populations. A linear fit to the model predictions shows that  $\text{Age} \propto \sigma^{0.58 \pm 0.02}$ , which is in excellent agreement with recent determination by Nelan et al. (2005), who found  $\text{Age} \propto \sigma^{0.59 \pm 0.13}$ . Fur-

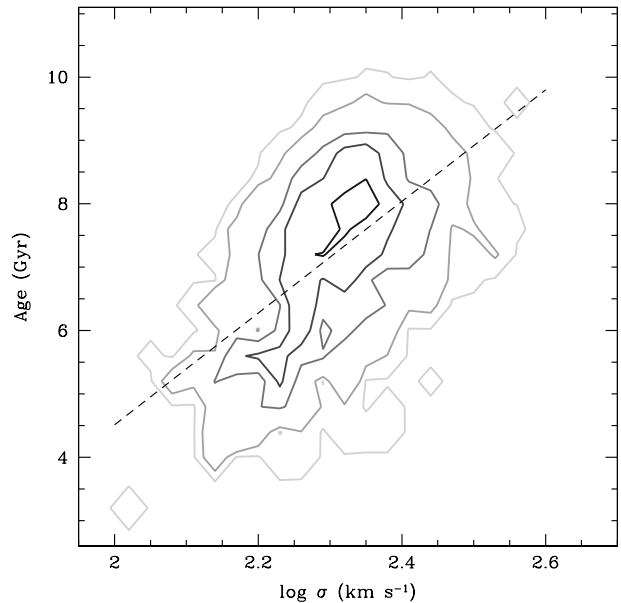


**Figure 5.** The  $r$ -band luminosity-weighted age of the stellar population as a function of the velocity dispersion predicted by GALFORM. The model galaxies are at redshift  $z = 0.13$  and are selected in a similar way to the observational sample of Ber05. The contours indicate the abundance of model galaxies, with darker lines corresponding to a higher number density. The dashed line shows the best fit to the model predictions.

thermore, we verify that the inclusion of AGN feedback, as implemented by Bower et al. (2006), does not change this relation substantially, giving  $\text{Age} \propto \sigma^{0.51 \pm 0.03}$ . At first sight, these predictions seem to contradict those presented, for a different observational selection, by Nagashima et al. (2005b). However, it is important to note that, at least in the case of the model galaxies, the slope and scatter of the Age –  $\sigma$  relation is very sensitive to the selection criteria applied.

### 4.3 Radius-Luminosity Relation

Another component of the fundamental plane of early-type galaxies is the relation between radius and luminosity; galaxies with larger radii are more luminous. This was originally of interest for use in distance scale measurements and cosmological tests (Sandage & Perelmuter 1990). Different studies indicate that this relation varies slightly with wavelength. For example, Schade et al. (1997) determined  $L_B \propto r_e^{1.33}$  in the B-band and Pahre et al. (1998) found  $L_K \propto r_e^{1.76}$  in the K-band. For SDSS early-type galaxies, Bernardi et al. (2003b) reported  $L_g \propto r_e^{1.50}$  in the g-band and  $L \propto r_e^{1.58}$  in the r, i and z-bands, which is consistent with the variation of slope with wavelength suggested by the earlier determinations.

We compare the predicted radius-luminosity relation with the Ber05 data in Fig. 6. The effective radius plotted here,  $r_e$ , is the projected bulge half-light radius, which is related to the half-mass radius in 3D,  $r_b$ , by:  $r_e = r_b/1.35$ . The model predictions do not change if we compute a composite half-mass (half-light) radius from the disk and bulge

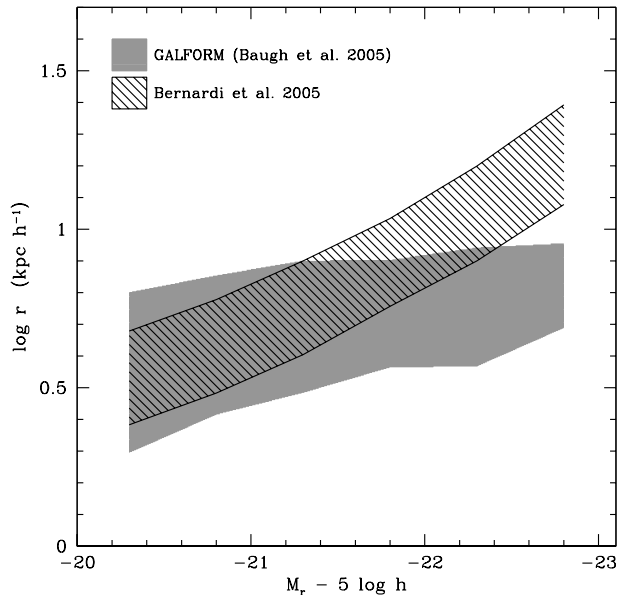


**Figure 6.** The relation between half-light radius and r-band magnitude for early-type galaxies. Again, the predictions for GALFORM galaxies are shown in gray and the hatched shaded distribution represents the SDSS sample; in both cases the shading shows the 10 to 90 percentile range.

components of the galaxy, as the model galaxies we consider are bulge dominated. The slope of the predicted radius-luminosity relation is flatter than is observed. The agreement between the model predictions and the observations is best at fainter magnitudes; the brightest early-type galaxies are predicted to be around a factor of three smaller in effective radius than is observed. Fig. 6 and Fig. 3 suggest that in the model, the high luminosity early-type galaxies have a pseudo-angular momentum which is lower than would be inferred from the data (see § 2.2 for the definition of the pseudo-angular momentum of a spheroid). This lack of pseudo-angular momentum could be traced back to the feedback processes used in the model (see for example Fig. 8 of Cole et al. 2000, which shows the impact on the predictions for the distribution of disk scalelengths when the strength of supernova feedback is varied). However, as we shall see later, we find similar results when using the Bower et al. model, in which a different form of feedback is effective in more massive dark haloes from that used in the Baugh et al. model.

The evolution of the radius-luminosity relation with redshift is plotted in Fig. 7. We find no clear change in the slope of the radius-luminosity relation over this redshift interval, in agreement with the results of Bernardi et al. (2003b). We shall return to this point in section 5.

#### 4.4 Effective Mass

We can define an effective dynamical mass,  $M_{\text{dyn}}$ , by setting  $M_{\text{dyn}} \equiv r_e \sigma^2 / G$ . This differs from the true mass,  $M$ , because the definition of  $M_{\text{dyn}}$  ignores any rotational support and the flattening of galaxies. The difference between the two masses can be quantified by a correction term,  $\xi$ :

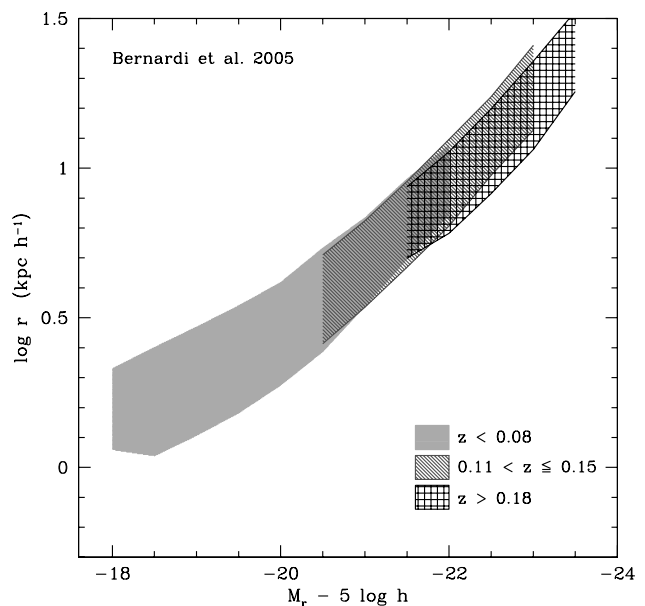
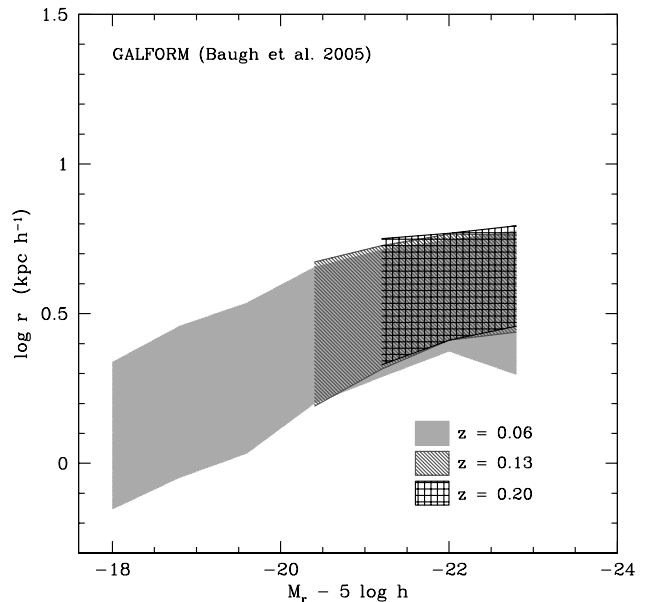


**Figure 7.** The evolution with redshift of the radius - r-band luminosity relation. The upper panel shows GALFORM galaxies at the median redshifts of the observational subsamples:  $z = 0.06$ ,  $z = 0.13$  and  $z = 0.20$ . The lower panel shows the results for the Bernardi et al. (2005) sample divided into volume-limited bins, as indicated by the legend.

$M = \xi M_{\text{dyn}}$ . For a galaxy with T-type E0, there is no flattening or rotational support and so  $\xi = 1$ . In contrast, for the case of an E6 galaxy, the true mass is almost twice as large as the dynamical mass, with  $\xi \sim 1.9$  (see Bender et al. 1992, for details).

In Fig. 8 we compare our prediction for the relation between dynamical mass and luminosity with the observed result for the Bernardi et al. (2005) sample. The figure reveals reasonable agreement between the model and observations. For the model we find,  $L_r \propto (r_e \sigma^2)^{1.22 \pm 0.04}$ , which is

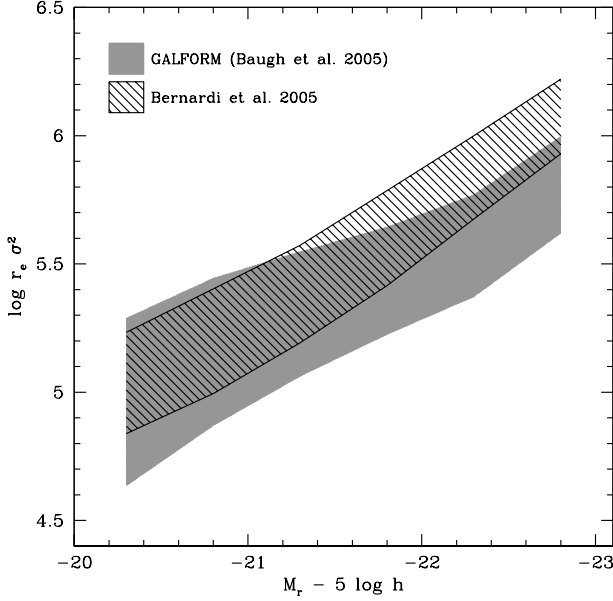


**Figure 8.** The relation between dynamical mass and luminosity. The GALFORM data is represented in gray and the dark hatched shaded region represents the Bernardi et al. (2005) sample. The shading connects the 10 and 90 percentile values.

slightly different from the result of Bernardi et al. (2003b),  $L_r \propto (r_e \sigma^2)^{0.87}$ . As we noted when discussing the radius-luminosity relation, high luminosity galaxies in the model display a lower specific pseudo-angular momentum than is observed, which translates into a smaller dynamical mass.

#### 4.5 Fundamental Plane

Observational studies indicate that early-type galaxies show tight correlations between their kinematic and photometric properties (Djorgovski & Davis 1987; Dressler et al. 1987). The remarkably small scatter about the so-called fundamental plane connecting the effective radius, velocity dispersion and surface brightness of early types encodes information about the formation and evolution of these galaxies.

The existence of a fundamental plane is expected if a stellar system obeys the virial theorem, which connects the kinetic and potential energies. The assumption of virial equilibrium gives a relation between the three-dimensional velocity dispersion,  $\sigma_{3D}$  and the “gravitational” radius,  $r_g$ , assuming that the system is gravitationally bound:

$$\sigma_{3D}^2 = \frac{GM}{r_g}. \quad (4)$$

This equation can be rewritten in terms of the central one dimensional velocity dispersion,  $\sigma_{1D}$ , and the effective radius of the galaxy,  $r_e$ ,

$$\sigma_{1D}^2 = \frac{GM}{\psi_r \psi_v r_e}, \quad (5)$$

where we have defined structural constants such that

$$\psi_v \equiv \frac{\sigma_{3D}^2}{\sigma_{1D}^2}, \quad \psi_r \equiv \frac{r_g}{r_e}.$$

based on the assumption that the population is homologous.

The mean surface brightness within half-mass radius of a galaxy is  $I_e \equiv L/2\pi r_e^2$ , where  $L$  is the total luminosity of the galaxy and the mean surface density is given by  $\Sigma_e \equiv M/2\pi r_e^2$ . The ratio of the surface brightness to the surface density is equal to the mean mass-to-light ratio of the galaxy, within  $r_e$ :  $\Sigma_e/I_e = M/L$ . Using these definitions, Eq. 5 can be rearranged to give an expression for the fundamental plane,

$$r_e = \frac{\psi_r \psi_v \sigma_{1D}^2}{2\pi G I_e (M/L)},$$

$$\log r_e = 2 \log \sigma + 0.4 \mu_e + \log(\psi_r \psi_v) - \log(M/L) + \gamma, \quad (6)$$

where  $\gamma$  is a constant whose value depends upon  $G$  and the choice of units.

The observed plane is slightly different from the form predicted in Eq. 6, which follows by applying the virial theorem to a purely stellar galaxy without any dark matter and assuming an homologous population. For example, Jørgensen et al. (1996) found  $\log r_e = 1.24 \log \sigma + 0.328 \mu_e + \gamma'$ , while Bernardi et al. (2003c) obtained  $\log r_e = (1.49 \pm 0.05) \log \sigma + (0.30 \pm 0.01) \mu_e - (8.78 \pm 0.02)$ .

The discrepancy between the theoretical prediction outlined above and the observational results is known as the tilt of the fundamental plane. Trujillo et al. (2004) argued that this tilt is due to a combination of effects: structural non-homology, which means a change in the surface brightness profile of the early-types with luminosity, and a variation in the mass-to-light ratio of the stellar populations with galaxy luminosity.

The intrinsic thickness or scatter in the fundamental plane poses another challenge, and the interpretation is far from clear. Forbes et al. (1998) showed that the scatter was mainly due to the age of the stellar population. However, Pahre et al. (1999) demonstrated that the position of the galaxy relative to the FP could not be entirely due to age or metallicity effects.

To determine the location of the fundamental plane, we consider an orthogonal fit to the plane given by:

$$\log r_e = a \log \sigma + b \mu_e + c,$$

and determine the values of the coefficients  $a$ ,  $b$  and  $c$  by minimizing the quantity

$$\delta = \sum_{i=1}^N \frac{(\log r_{e,i} - a \log \sigma_i - b \mu_{e,i} - c)^2}{1 + a^2 + b^2}$$

Following this procedure, we obtain a fundamental plane for GALFORM given by  $\log r_e = (1.94 \pm 0.01) \log \sigma + (0.19 \pm 0.01) \mu_e - (7.54 \pm 0.03)$  in the r-band.

In Fig. 9, we plot the fundamental plane derived from GALFORM model galaxies, along with the data from Bernardi et al. (2005) in the same projection of the plane. Fig. 9 reveals excellent agreement between the fundamental plane predicted by GALFORM and the observational data: we can reproduce not only the tilt, but also the scatter associated with the plane. In the g-band we calculate:  $\log r_e = (2.12 \pm 0.02) \log \sigma + (0.19 \pm 0.01) \mu_e - (7.92 \pm 0.07)$ ; and similar results in the i and z-bands. This reveals that the slope of the FP is independent of wavelength, analogous to the results found by Bernardi et al. (2003c).

We plot the fundamental plane at different redshifts in Fig. 10. The radius, velocity dispersion, surface brightness



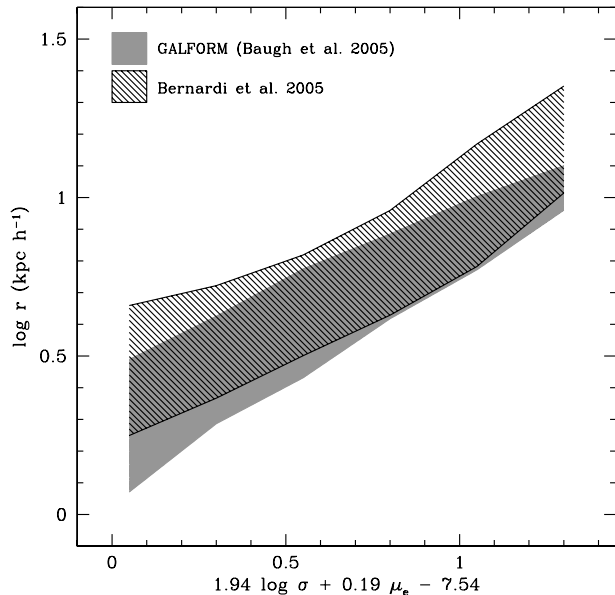


**Figure 9.** The fundamental plane for GALFORM early-type galaxies (gray shading) compared with the observational data from Ber05 (hatched shading). The shading denotes the 10 to 90 percentile interval.

and mass-to-light ratios of the model galaxies all evolve with time (see §5), so one might expect to see some evolution in the fundamental plane itself, unless the changes in these quantities occur in such a way as to cancel out any evolution in the locus of the plane. Ber05 report evolution in the position of the fundamental plane which corresponds to a change in the mean galaxy surface brightness of  $\Delta\mu_e \approx -2z$ . We find no clear evidence for evolution in the model predictions over the same redshift interval. In the next section we show the predictions for the scaling relations over a wider baseline in redshift.

## 5 THE EVOLUTION OF SCALING RELATIONS

We now present the GALFORM predictions for the evolution of the structural and photometric properties of early-type galaxies with redshift. In this section, we consider the evolution over a much wider baseline in redshift than we addressed in the previous section. Furthermore, in order to get a clear picture of the nature of the evolution, we relax some of the selection criteria which we applied to the model output in previous sections, where the goal was to mimic the Ber05 sample selection as closely as possible. The only selection we apply in this section is that the bulge must account for at least 80% of the total luminosity in the rest-frame  $r$ -band.

It is important to be able to disentangle changes in the typical stellar populations of early-type galaxies with redshift from evolution in their structural properties. Hence, we first examine the predicted evolution in the mass-to-light ratio of early-type galaxies in Fig. 11. The stellar pop-

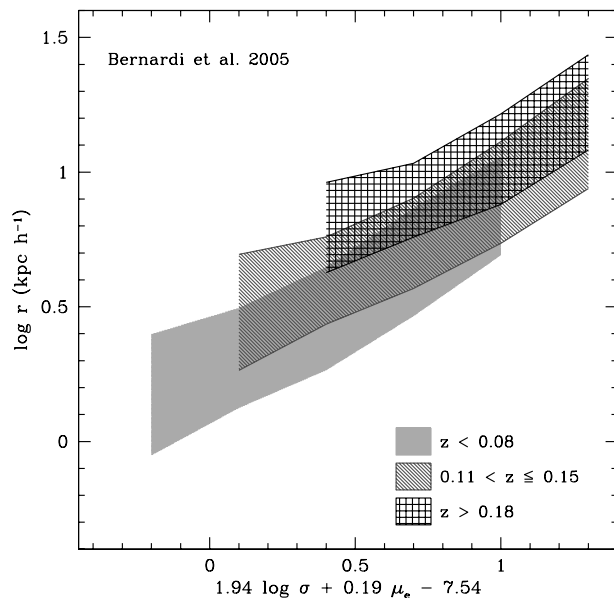
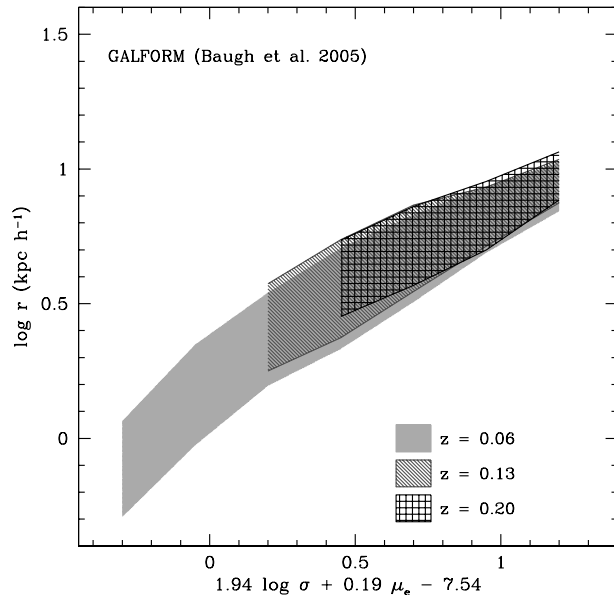


**Figure 10.** The evolution of the fundamental plane with redshift. The upper panel shows model predictions for redshifts  $z = 0.06$ ,  $z = 0.13$  and  $z = 0.20$ ; these are the median redshifts of the observational samples plotted in the lower panel. Again, the shaded regions show the 10 to 90 percentile ranges of the distributions.

ulations of early-type galaxies at  $z = 1$  in GALFORM have lower mass-to-light ratios by a factor of  $\approx 3$  compared with the early-types at  $z = 0$ . This is in excellent agreement with the change in mass-to-light ratio in the  $r$ -band inferred from observations by van der Ven et al. (2003) (see also van der Wel et al. 2005; Treu et al. 2005).

The evolution with redshift of the Faber-Jackson relation is shown in Fig. 12. We show the correlation between velocity dispersion and the  $r$ -band magnitude in the rest-frame for the local universe ( $z = 0$ ),  $z = 0.5$  and  $z = 1$ . Fig. 12 shows that the model predicts differential evolution

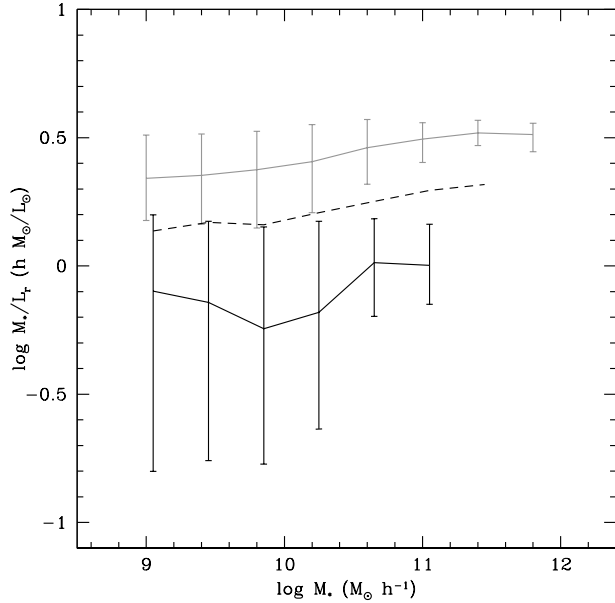


**Figure 11.** The predicted evolution with redshift of the mass-to-light ratio in the rest-frame  $r$ -band, plotted against the stellar mass. The grey line shows the prediction for  $z = 0$ , the dashed line for  $z = 0.5$  and the solid black line for  $z = 1$ .

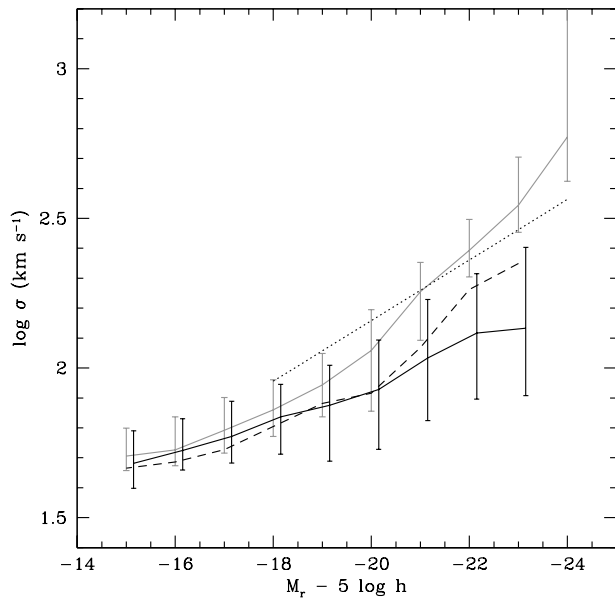


**Figure 12.** The predicted evolution with redshift of the relation between velocity dispersion and rest-frame  $r$ -band luminosity. The grey solid line shows the Faber-Jackson relation in the local universe ( $z = 0$ ), while the short-dashed line shows it at  $z = 0.5$  and the black solid line at  $z = 1$ . The errorbars show the 10 to 90 percentile range of the distribution. The dotted line shows the observed low redshift Faber-Jackson relation for SDSS early-type galaxies for reference (Bernardi et al. 2003b).

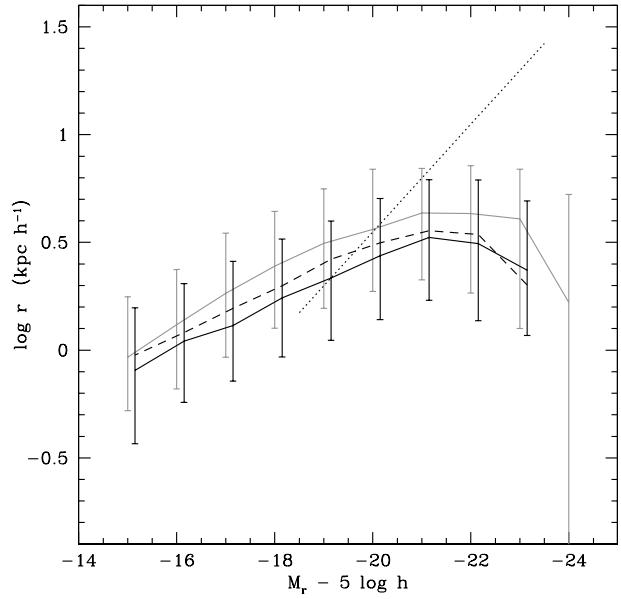


**Figure 13.** The predicted evolution with redshift of the relation between radius and luminosity. The grey solid line shows the relation in the local universe, the black dashed line at  $z = 0.5$  and the black solid line at  $z = 1$ . The errorbars show the 10 to 90 percentile range of the model predictions. The dotted line represents the relation for SDSS early-type galaxies for reference (Bernardi et al. 2003b).

in velocity dispersion with rest-frame luminosity; at brighter luminosities, the velocity dispersion drops by up to a factor of  $\approx 3$  between  $z = 0$  and  $z = 1$ , whereas for fainter luminosities, the change in velocity dispersion is much more modest. There are two competing evolutionary trends which cancel one another out to differing degrees depending upon galaxy luminosity. First, the age of the stellar population drops with increasing redshift, leading to a brightening of the galaxy at a fixed velocity dispersion. This occurs because we have restricted our attention to early-type galaxies, whose stellar populations are, on the whole, evolving passively (see Fig. 11). Second, extrapolating the trend seen in the Age  $-\sigma$  relation in the model at  $z = 0$  (see Fig. 5), we might expect to see a reduction in velocity dispersion with increasing redshift. This is because at higher redshifts we are looking at galaxies with younger stellar populations, and we have shown that, at  $z = 0$ , younger galaxies tend to have lower velocity dispersions. We note that the scatter around the FJ relation seems to increase slightly with redshift. Our predictions for bright galaxies are in good agreement with the evolution in the FJ relation reported for early-type galaxies in the K20 survey by di Serego Alighieri et al. (2005).

Fig. 13 shows how the relation between radius and luminosity varies with redshift. The primary agent behind the shift in the predictions is the passive evolution of the stellar populations in the elliptical galaxies. As redshift increases, we see the bulk of the stars in ellipticals when they were younger and hence brighter. There is no significant trend in the size of the scatter in this relation with redshift.

Holden et al. (2005) estimated the evolution in the sur-

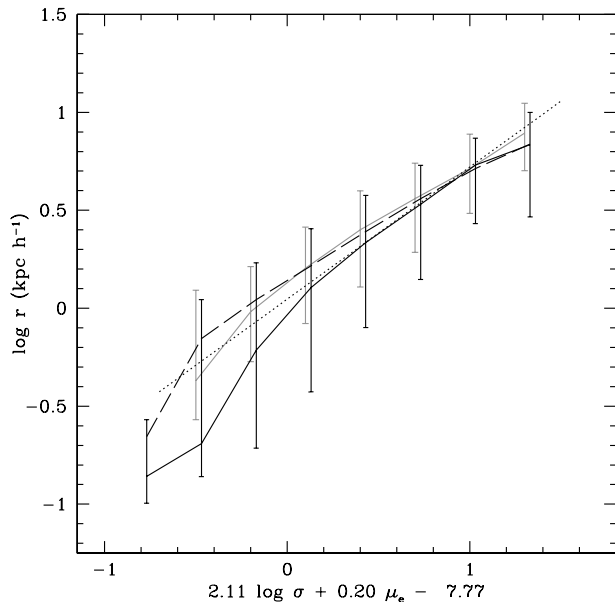


**Figure 14.** The predicted evolution of the fundamental plane with redshift. The grey solid line shows the relation in the local universe, the dashed black line at  $z = 0.5$  and the black solid line at  $z = 1$ . The errorbars show the 10 to 90 percentile range of the model predictions. The dotted line is a fit to Bernardi et al. (2005) data for reference.

face brightness - galaxy size relation using early-type galaxies in clusters at  $z \sim 1$ . These authors found that the zero-point of the relation brightens by about 1.25 in the rest-frame B-band for cluster galaxies over the redshift interval  $z = 0-1$ ; this is comparable, though somewhat smaller, to the amount of evolution we predict in Fig. 13 for all ellipticals, without restricting our attention to cluster galaxies.

The evolution of the fundamental plane has long been used to study changes in the stellar populations of galaxies (e.g. van Dokkum & Franx 1996; van Dokkum et al. 2001; Gebhardt et al. 2003; van der Wel et al. 2006). As previously noted, Bernardi et al. (2003c) found evolution in the fundamental plane which is consistent with the passive aging of the stellar population,  $\Delta\mu_e \approx -2z$ , but without any noticeable difference in the slope. There is a general consensus in the literature regarding the nature of the evolution of the fundamental plane (Gebhardt et al. 2003; Ziegler et al. 2005; Jørgensen et al. 2006). We plot the model predictions in the  $z = 0$  GALFORM fundamental plane (Fig. 14),  $\log r_e = (2.11 \pm 0.02) \log \sigma + (0.20 \pm 0.01)\mu_e - (7.77 \pm 0.07)$  (note that the projection of the fundamental plane is different in this section from the previous one due to the different selection applied to the model galaxies). In this projection, we find no evolution in the slope or offset of the fundamental plane up to  $z = 1$ , which is contrary to claims made from observations. This could imply that there is too much recent star formation in elliptical galaxies in the model. Baugh et al. (1996) show that in a model with a similar parameterisation of the star formation timescale in quiescent disks to the one used in Baugh et al. (2005), major mergers which occur at low redshift could produce a small amount of stars in a burst. The stars formed in such a burst contribute

little to the total stellar mass of the bulge but can affect the luminosity of the galaxy.

An interesting aspect, which will be analysed in the next section, is that the amount of scatter around the fundamental plane clearly evolves with increasing redshift.

## 6 THE DEPENDENCE OF THE STRUCTURAL PROPERTIES OF ELLIPTICALS ON THE PHYSICAL INGREDIENTS OF THE MODEL

Our calculation of the sizes of galactic spheroids contains several steps and is sensitive to some of the physical ingredients of the galaxy formation model more than others. The beauty of semi-analytical modelling is that we can switch off or vary particular assumptions or processes to isolate their impact on the model predictions. Such a study is only possible to a very limited extent in fully numerical simulations of galaxy formation. Moreover, the high speed of the semi-analytical calculations compared with a numerical simulation allows us to examine many different variants in a short time. In this section, we seek to establish the sensitivity of our model predictions for the structural and photometric properties of spheroids to the composition of the model. For this purpose, we study the model predictions at  $z = 0$  and consider bulge dominated galaxies, i.e. those with a bulge-to-total luminosity ratio in the  $r$ -band of  $B/T > 0.8$ . The results of this section are presented in Figs. 15, 16, 17 and 18, which look, respectively, at how deviations from the fundamental plane correlate with various galaxy properties, the Faber-Jackson relation between velocity dispersion and luminosity, the radius-luminosity relation and the fundamental plane.

### 6.1 The scatter around the fundamental plane

In the previous section we noted that the size of the deviations from the zero-point of the fundamental plane (FP) increase with redshift. This suggests that the scatter around the projection of the fundamental plane can be, in part, due to differences in the formation epoch of galaxies. Fig. 15 shows how the deviation from the fundamental plane correlates with various galaxy properties. Here, the quantity  $\Delta$  represents the residuals from the  $z = 0$  model fundamental plane:  $\Delta = \log r_b - \log r_{\text{fit}}$ , where  $\log r_{\text{fit}}$  represents a linear fit to the fundamental plane. Fig. 15(a) reveals a strong anticorrelation between the scatter and the  $r$ -band luminosity-weighted age of the galaxy, in the sense that galaxies which lie above the fundamental plane are younger. This strong correlation indicates that the age of the stellar population plays an important role in determining the position of the galaxy in the fundamental plane space, where the mean FP relation is defined mainly by early-type galaxies with luminosity weighted ages around  $\sim 10$  Gyr (see Forbes et al. 1998; Pahre et al. 1999). Contrary to Bernardi et al. (2003b), we find that the residuals are correlated with  $r$ -band absolute magnitude, but not with  $g-r$  colour (Fig. 15(b) and (c), respectively). Interestingly, we see in Fig. 15(d) that the absolute metallicity of the stellar population is anticorrelated with the scatter from the fundamental plane: metal-rich galaxies are to be found predominantly below the mean fundamental plane relation. There is

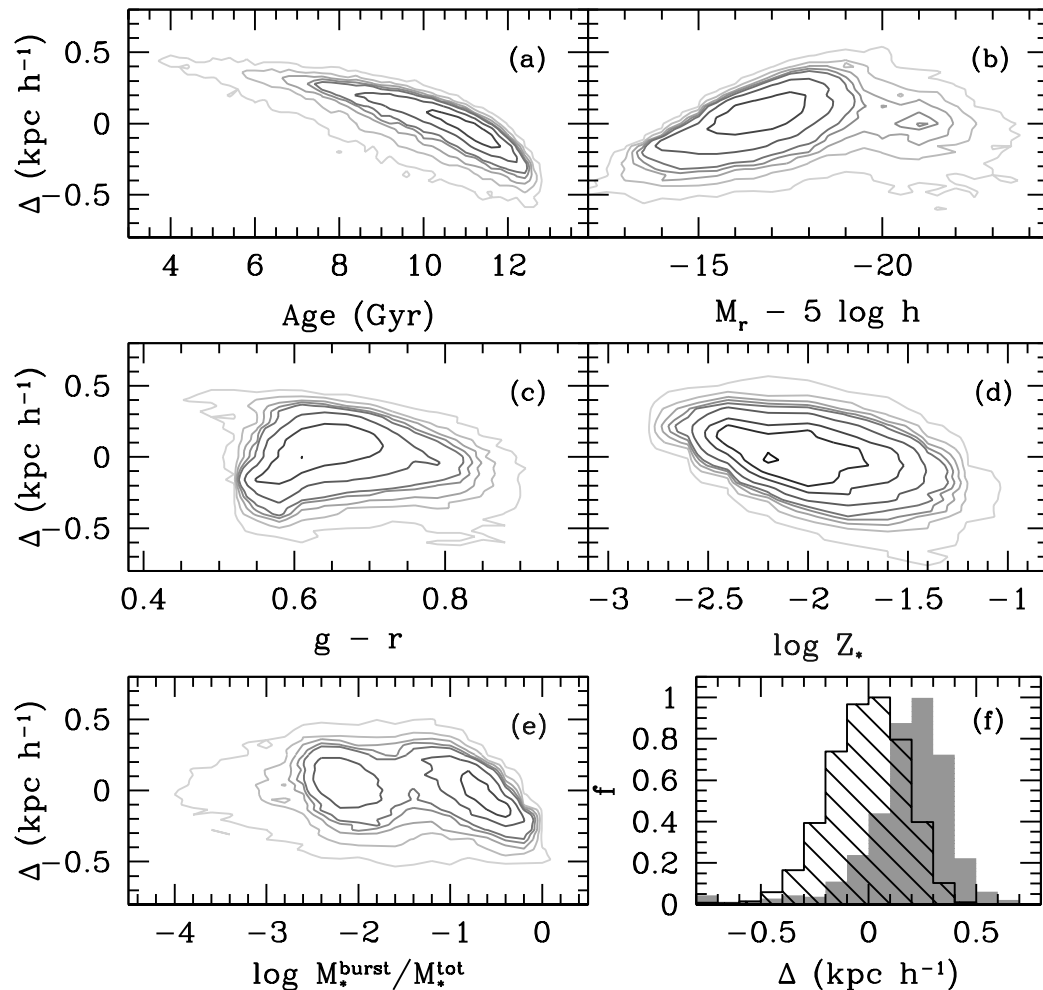


**Figure 15.** The dependence of the deviation (defined as  $\Delta = \log r_e - \log r_{\text{fit}}$ , where  $\log r_{\text{fit}}$  represents a linear fit) from the fundamental plane in the model on various galaxy properties: (a) the  $r$ -band luminosity-weighted age, (b) the  $r$ -band absolute magnitude, (c) the  $g - r$  colour, (d) the stellar metallicity, (e) the ratio between the mass of the stars formed in the last burst,  $M_*^{\text{burst}}$ , and the total stellar mass,  $M_*^{\text{tot}}$ , at the present day; and (f) whether or not the galaxy is a central galaxy or a satellite. The contours are indicative of the density of model galaxies. In the panel (f), the hatched histogram represents the scatter from the fundamental plane for the central galaxies, and the grey histogram shows the distribution for the satellite galaxies.

little correlation between the residuals from the fundamental plane and the fraction of the total stellar mass formed in the last burst of star formation triggered by a galaxy merger, until this fraction exceeds 10% (Fig. 15(e)); galaxies in which this fraction is higher lie below the FP. The importance of the burst tends to increase with the lookback time, which implies that this would be another manifestation of the correlation between residuals and luminosity weighted age. In Fig. 15(f), we show the distribution of the residuals for central and satellite galaxies. It is clear that satellite galaxies tend to lie above the fundamental plane relation. Although not plotted in Fig. 15, we find no important relations between the halo properties, such as mass or circular velocity, and the scatter from the FP. We do find, however, a weak correlation between the scatter and the pseudo-specific angular momentum of the bulge: galaxies with smaller angular

momentum are to be found predominantly below the fundamental plane relation. This shows that departures from the FP are also caused by feedback processes in galaxies.

## 6.2 The physics of the model and the scaling relations

The first ingredient we test is the adiabatic contraction model used to take into account the gravitational pull of the baryons on the dark matter. To recap, the condensation of baryons at the centre of the dark matter halo provides an additional gravitational force on the dark matter which causes it to move inwards, thereby increasing the density of dark matter in the central part of the halo. This in turn alters the gravitational force on the baryons due to the dark matter. The degree of contraction is computed by

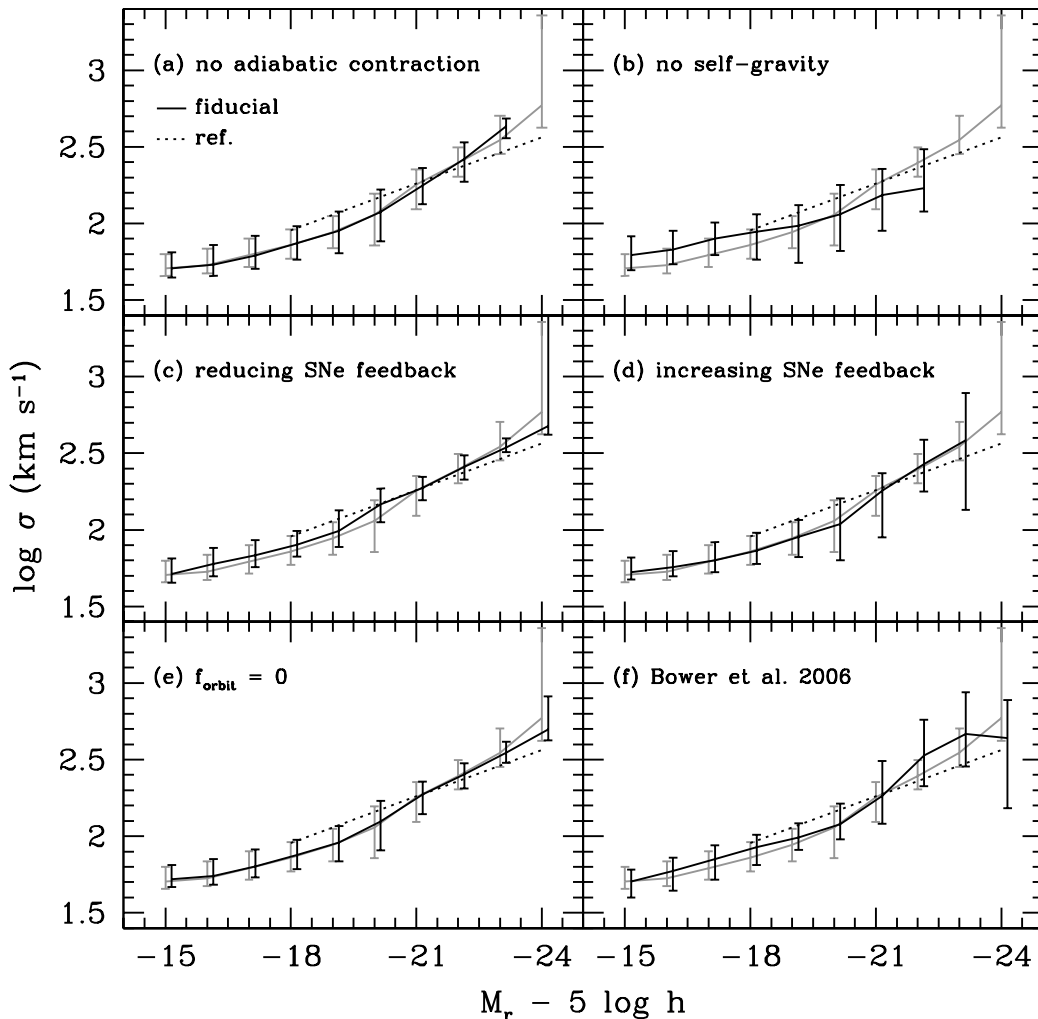


**Figure 16.** The sensitivity of the model predictions for the Faber-Jackson relation to: (a) switching off adiabatic contraction, (b) omitting the self-gravity of the baryons, (c) reducing the strength of supernova feedback, (d) increasing the strength of SNe feedback, (e) the omission of the orbital energy from the calculation of the size of the merger remnant and (f) using the Bower et al. (2006) model with AGN feedback. In each panel, the grey line shows the median prediction from the reference model (Baugh et al. 2005), at  $z = 0$ . The black solid line shows the median for the variant model. The errorbars indicate the 10 to 90 percentile of the predictions. The dotted line in each panel shows the observed relation for SDSS early-type galaxies for reference (Bernardi et al. 2003b).

exploiting the fact that, in a slowly varying potential, the action integral,  $\oint p_i dq_i$ , is an adiabatic invariant for each particle of mass  $i$ , where  $p_i$  is the conjugate momentum of the coordinate  $q_i$  (Barnes & White 1984; Blumenthal et al. 1986; Jesseit et al. 2002). If we assume spherical symmetry and circular orbits, the action integral simplifies to the conservation of angular momentum in spherical shells,  $rM(r)$ . The adiabatic contraction of the dark matter leads to a more centrally peaked halo density. The main consequence of switching off the adiabatic contraction of the dark matter halo is that the half-mass radius of the spheroid increases (Fig. 17(a)). The radii of bright galaxies increase by a larger factor than those of faint galaxies, leading to a steepening of the radius-luminosity relation. The slope of the radius-luminosity is in much better agreement with the observed

slope on omitting adiabatic contraction, although the model galaxies are too large overall (both spheroids and disks).

Next we ignore the self-gravity of the baryons when computing the size and effective rotation speed of the disk and bulge. This also means that there is no adiabatic contraction. The rotation curve of the galaxy in this case is set purely by the dark matter, which is assumed to have an NFW density profile (Navarro, Frenk, & White 1997). The consequences of this change are a flattening in the velocity dispersion-luminosity relation (Fig. 16(b)), with brighter galaxies displaying a lower velocity dispersion, and a uniform increase in the radius of the spheroid (Fig. 17(b)). In combination, these changes result in a different projection of the fundamental plane which looks flatter in the projection which best fits the predictions of the fiducial model.

Feedback, the regulation of the star formation rate due

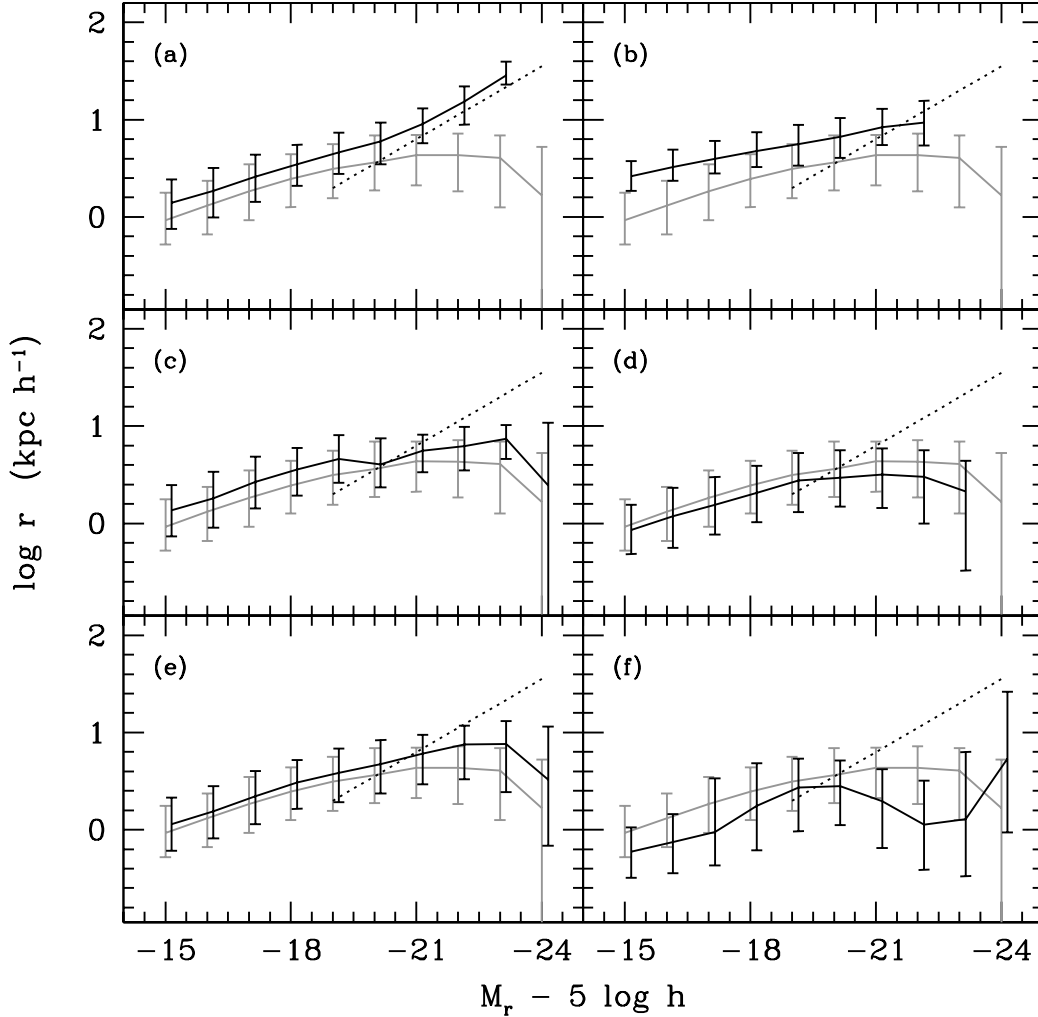


**Figure 17.** The sensitivity of the relation between radius and luminosity to: (a) switching off adiabatic contraction, (b) omitting the self-gravity of the baryons, (c) reducing the strength of supernova feedback, (d) increasing the strength of SNe feedback, (e) the omission of the orbital energy from the calculation of the size of the merger remnant and (f) using the Bower et al. (2006) model with AGN feedback. In each panel, the grey line shows the median prediction from the reference model (Baugh et al. 2005), at  $z = 0$ . The black solid line shows the median for the variant model. The errorbars indicate the 10 to 90 percentile of the predictions. The dotted line in each panel shows the observed relation for SDSS early-type galaxies for reference (Bernardi et al. 2003b).

to the reheating and ejection of cooled gas following the injection of energy into the interstellar medium by supernova explosions, plays an important role in setting the sizes of disk galaxies (Cole et al. 2000). The strength of SNe feedback is quantified in the model by the parameter  $\beta$  (for details see Cole et al. 2000):  $\beta = (V_{\text{hot}}/V_{\text{disc}})^{\alpha_{\text{hot}}}$ , where  $V_{\text{hot}}$  and  $\alpha_{\text{hot}}$  are parameters and  $V_{\text{disc}}$  is the rotation speed of the disc at the half mass radius. The mass of cold gas which is reheated is given by  $\dot{M}_{\text{reheat}} = \beta\psi$ , where  $\psi$  is the star formation rate. In the Baugh et al. model, the values adopted for these parameters are:  $\alpha_{\text{hot}} = 2$  and  $V_{\text{hot}} = 300 \text{ km s}^{-1}$ . We show the impact of reducing (by setting  $v_{\text{hot}} = 100 \text{ km s}^{-1}$ ) and increasing (by setting  $v_{\text{hot}} = 600 \text{ km s}^{-1}$ ) the strength of supernova feedback in Figs. 16, 17 and 18-(c)-(d). Cole et al. demonstrated that increasing the strength of supernova feedback results in gas cooling to form stars in larger

haloes, which leads to larger disks. Conversely, reducing the feedback allows gas to cool and form stars in smaller haloes resulting in smaller disks. These trends are reproduced in Figs. 17(c) and (d). There is little change in velocity dispersion on changing the strength of the supernova feedback. The shift in the zeropoint of the radius luminosity relation produces a change in the location of the fundamental plane (see Fig. 18-(c)-(d)).

In the fiducial GALFORM model, spheroids are the end products of galaxy mergers. As we explained in § 2, the radius of the merger remnant is determined by conserving the binding energy of the individual galaxies involved in the merger and their relative orbital energy. The contribution of the orbital energy to the energy budget is parameterized by  $f_{\text{orbit}}$ : the standard choice is to set  $f_{\text{orbit}} = 1$  and to include the full orbital energy in the calculation of the remnant size.

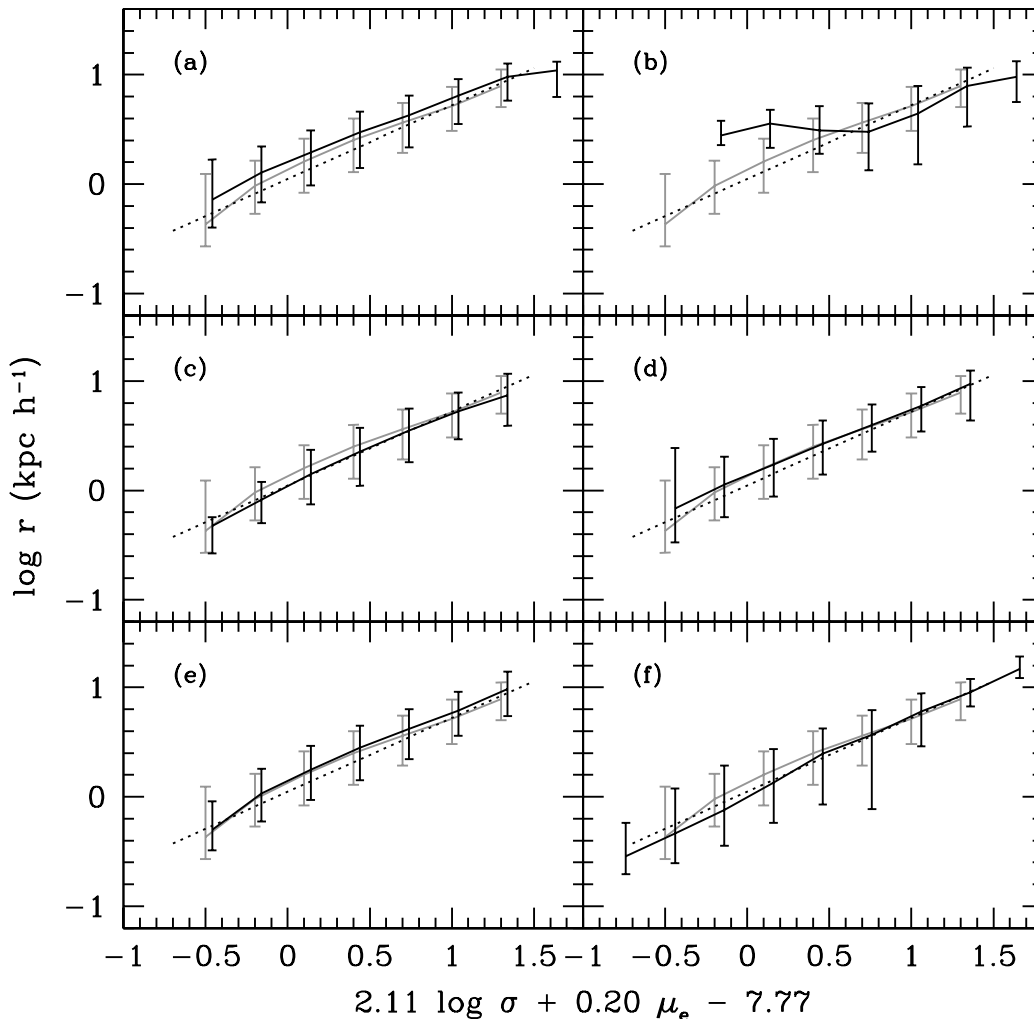


**Figure 18.** The sensitivity of the fundamental plane to: (a) switching off adiabatic contraction, (b) omitting the self-gravity of the baryons, (c) reducing the strength of supernova feedback, (d) increasing the strength of SNe feedback, (e) the omission of the orbital energy from the calculation of the size of the merger remnant and (f) using the Bower et al. (2006) model with AGN feedback. In each panel, the grey line shows the median prediction from the reference model (Baugh et al. 2005), at  $z = 0$ . The black solid line shows the median for the variant model. The errorbars indicate the 10 to 90 percentile of the predictions. The dotted line in each panel shows the observed relation for SDSS early-type galaxies for reference (Bernardi et al. 2005).

In Figs. 16, 17 and 18-(e), we show the effect of removing the contribution of the orbital energy from the calculation of the radius of the spheroid produced by mergers, i.e. we set  $f_{\text{orbit}} = 0$ . Perhaps surprisingly, this change results in an imperceptibly small change in the radius of the spheroid, except in the case of the brightest galaxies.

Finally we consider the model of Bower et al. (2006), who implemented an AGN feedback scheme into *GALFORM*, in which cooling flows are quenched in massive haloes at low redshift. As a result of this change to the cooling model in *GALFORM*, Bower et al. (2006) were able to produce improved matches to the local B and K-band luminosity functions, the bimodality of colour distribution and the evolution of the stellar mass function. In Figs. 16, 17 and 18-(f) we plot the scaling relations for Bower et al. (2006) model. Though the model performs quite well in reproducing the local funda-

mental plane of early-type galaxies and the Faber-Jackson relation, the radius-luminosity relation for bright galaxies is substantially different from observations and from the Baugh et al. (2005) model: the luminous galaxies are up a factor of three smaller in radius.

## 7 DISCUSSION AND CONCLUSIONS

We presented tests of the model proposed by Cole et al. (2000) to calculate the scale sizes of the disk and bulge components of galaxies. This is currently the most sophisticated model in use in semi-analytical models for computing the radii of galaxies. In brief, the model assumes that galactic disks have an exponential profile and that spheroids follow an  $r^{1/4}$  law in projection. The hot gas atmosphere in dark

matter haloes is assumed to have the same specific angular momentum as the dark matter. Gas is assumed to retain its angular momentum as it cools to form a galactic disk. The size of a merger remnant is computed by conserving the sum of the binding and orbital energies of the merging galaxies and applying the virial theorem. The self-gravity of the baryons and their impact on the distribution of dark matter in the central parts of the halo are taken into account. Cole et al. demonstrated that this model predicts scale length distributions for galactic disks which are in excellent agreement with observations.

In this paper, we carried out the first tests of the model predictions for the structural properties of early-type galaxies and the evolution of these relations with redshift. We also exploited the modular nature of semi-analytical models to vary or switch off various physical ingredients of the model in order to assess their influence on the model predictions.

The model enjoys some notable successes. We demonstrated that the model can match the abundance of early-type galaxies in the SDSS sample of Ber05. We can also reproduce the Faber-Jackson relation between velocity dispersion and luminosity and its evolution with redshift. Furthermore, we find a relation between velocity dispersion and age which is in excellent agreement with recent observations. Perhaps most impressively, the fundamental plane predicted by the model is in very good agreement with that inferred for SDSS early-types by Bernardi et al. (2003c). Also, the scatter from the FP reveals a strong correlation with age, luminosity and metallicity: galaxies that lie above the mean fundamental plane relation are younger, more luminous and metal-poor.

Nevertheless, despite these achievements, there are some model predictions which are at odds with the observations. Perhaps the most striking is the slope of the radius-luminosity relation; the model predicts a significantly flatter radius luminosity relation than is observed. Whereas the model predictions for the effective radii of faint spheroids are in good agreement with the data, the brightest galaxies are up to a factor of three smaller in the model. Our results suggest that, in the model, the brightest spheroids have less specific pseudo-angular momentum (this is a definition of convenience; see Section 2.2) than is the case for observed galaxies. This could be due to an underprediction of the effective mass of these galaxies or, could point to a deficiency in the modelling of feedback processes. Somewhat surprisingly, the predicted slope of the radius-luminosity relation is in much better agreement with the observations if the adiabatic contraction of the halo is switched off (although, in this case, the model galaxies are uniformly too large without adjusting other parameters). The adiabatic contraction of the halo in response to the presence of condensed baryons has been tested against numerical simulations (e.g. Jesseit et al. 2002; Sellwood & McGaugh 2005; Choi et al. 2006). Our prescription for computing the size of merger remnants could become inaccurate if there is a significant fraction of mass in the form of cold gas.

The other significant discrepancy is the evolution with redshift of the zero-point of the fundamental plane. The model predicts no evolution in the zero-point whereas observations show a shift consistent with passive evolution of the stellar populations of early-types. The model does predict a decline in the mass-to-light ratio of early-types with

increasing redshift, which is similar to that expected for the passive evolution of an old stellar population. However, the effective radii of galaxies also evolve with redshift in the model, to cancel out the expected shift in the zero-point of the fundamental plane from the change in the typical mass-to-light ratio.

In summary, the prescription outlined by Cole et al. for computing the radii of disks and bulges enjoys many successes, but displays a few important disagreements with observations. The solution of these remaining problems will require enhancement of the model of galaxy sizes, guided by the results of numerical simulations of the growth of disk galaxies and galaxy mergers (e.g. Okamoto et al. 2005; Robertson et al. 2006).

## ACKNOWLEDGEMENTS

CA gratefully acknowledges a scholarship from the FCT, Portugal. CMB is supported by the Royal Society. This research was partly supported by PPARC. We thank Andrew Benson and Richard Bower for allowing us to use results generated with the new version of the GALFORM code. We are grateful to Mariangela Bernardi for providing the observational data presented in this paper.

Funding for the SDSS and SDSS-II has been provided by the Alfred P. Sloan Foundation, the Participating Institutions, the National Science Foundation, the U.S. Department of Energy, the National Aeronautics and Space Administration, the Japanese Monbukagakusho, the Max Planck Society and the Higher Education Funding Council for England. The SDSS Web Site is <http://www.sdss.org/>.

The SDSS is managed by the Astrophysical Research Consortium for the Participating Institutions. The Participating Institutions are the American Museum of Natural History, Astrophysical Institute Potsdam, University of Basel, Cambridge University, Case Western Reserve University, University of Chicago, Drexel University, Fermilab, the Institute for Advanced Study, the Japan Participation Group, Johns Hopkins University, the Joint Institute for Nuclear Astrophysics, the Kavli Institute for Particle Astrophysics and Cosmology, the Korean Scientist Group, the Chinese Academy of Sciences (LAMOST), Los Alamos National Laboratory, the Max-Planck-Institute for Astronomy (MPA), the Max-Planck-Institute for Astrophysics (MPIA), New Mexico State University, Ohio State University, University of Pittsburgh, University of Portsmouth, Princeton University, the United States Naval Observatory and the University of Washington.

## REFERENCES

- Adelberger K.L., Steidel C.C., Shapley A.E., Pettini M., 2003, *ApJ*, 584, 45
- Barnes J., White S.D.M., 1984, *MNRAS*, 211, 753
- Baugh C.M., 2006, *Rep. Prog. Phys.*, submitted
- Baugh C.M., Lacey C.G., Frenk C.S., Granato G.L., Silva L., Bressan A., Benson A.J., Cole S., 2005, *MNRAS*, 356, 1191
- Baugh C.M., Cole S., Frenk C.S., 1996, *MNRAS*, 283, 1361
- Bender R., Burstein D., Faber S.M., 1992, *ApJ*, 399, 462
- Benson A.J., Bower R.G., Frenk C.S., Lacey C.G., Baugh C.M., Cole S., 2003, *ApJ*, 599, 38
- Benson A.J., Lacey C.G., Baugh C.M., Cole S., Frenk C.S., 2002, *MNRAS*, 333, 156
- Bernardi M., Sheth R.K., Nichol R.C., Schneider D.P., Brinkmann J., 2005, *AJ*, 129, 61



- Bernardi M., Sheth R.K., Annis J., et al., 2003a, *AJ*, 185, 1817  
Bernardi M., Sheth R.K., Annis J., et al., 2003b, *AJ*, 185, 1849  
Bernardi M., Sheth R.K., Annis J., et al., 2003c, *AJ*, 185, 1866  
Bernardi M., Sheth R.K., Annis J., et al., 2003d, *AJ*, 185, 1882  
Blumenthal G.R., Faber S.M., Flores R., Primack J.R., 1986, *ApJ*, 301, 27  
Bournaud F., Jog C. J., Combes F., 2005, *A&A*, 437, 69  
Bower R.G., Benson A.J., Malbon R., Helly J.C., Frenk C.S., Baugh C.M., Cole S., Lacey C.G., 2006, *MNRAS*, 370, 645  
Boylan-Kolchin M., Ma C., Quataert E., 2006, *MNRAS*, 369, 1081  
Choi J., Lu Y., Mo H.J., Weinberg M.D., 2006, astro-ph/0604587  
Cole S., Lacey C.G., Baugh C.M., Frenk C.S., 2000, *MNRAS*, 319, 168  
Cole S., Aragón-Salamanca A., Frenk C.S., Navarro J.F., Zepf S.E., 1994, *MNRAS*, 271, 781  
Connolly A.J., Szalay A.S., 1999, *ApJ*, 117, 2052  
De Jong R.S., Lacey C.G., 2000, *ApJ*, 545, 781  
Dekel A., Cox T.J., 2006, *MNRAS*, 370, 1445  
di Serego Alighieri S., et al., 2005, *A&A*, 442, 125  
Djorgovski S., Davis M., 1987, *ApJ*, 313, 59  
Dressler A., Lynden-Bell D., Burstein D., Davies R.L., Faber S.M., Terlevich R.J., Jackson R., 1987, *ApJ*, 313, 42  
Faber S.M., Jackson R., 1976, *ApJ*, 204, 668  
Forbes D.A., Ponman T.J., 1999, *MNRAS*, 309, 623  
Forbes D.A., Ponman T.J., Brown R.J.N., 1998, *ApJ*, 508, L43  
Gebhardt K., et al., 2003, *ApJ*, 597, 239  
Graham A. W., Driver S. P., Petrosian V., Conselice C. J., Ber-shady M. A., Crawford S. M., Goto T., 2005, *AJ*, 130, 1535  
Hatton S., Devriendt J.E.G., Ninin S., Bouchet F.R., Guiderdoni B., Vibert D., 2003, *MNRAS*, 343, 75  
Holden B.P., et al., 2005, *ApJ*, 626, 809  
Jesseit R., Thorsten N., Burkert A., 2002, *ApJ*, 571, L89  
Jørgensen I., Chiboucas K., Flint K., Bergmann M., Barr J., Davies R., 2006, *ApJ*, 639, L9  
Jørgensen I., Franx M., Kjærgaard P., 1996, *MNRAS*, 280, 167  
Kauffmann G., 1996, *MNRAS*, 281, 487  
Kobayashi C., 2005, *MNRAS*, 361, 1216  
Kormendy J., 1977, *ApJ*, 218, 333  
Lemson G., Virgo Consortium, 2006, astro-ph/0608019  
Malbon R.K., Baugh C.M., Frenk C.S., Lacey C.G., 2006, *MNRAS*, submitted, astro-ph/0607424  
Nagashima M., Lacey C.G., Okamoto T., Baugh C.M., Frenk C.S., Cole S., 2005b, *MNRAS*, 363, 31  
Nagashima M., Lacey C.G., Baugh C.M., Frenk C.S., Cole S., 2005a, *MNRAS*, 358, 1247  
Navarro J., Frenk C., White S., 1997, *ApJ*, 490, 493  
Nelán J.E., Smith R.S., Hudson M.J., Wegner G.A., Lucey J.R., Moore S.A.W., Quinney S.J., Suntzeff N.B., 2005, *ApJ*, 632, 137  
Okamoto T., Eke V.R., Frenk C.S., Jenkins A., 2005, *MNRAS*, 363, 1299  
Pahre M.A., Djorgovski S.G., de Carvalho R.R., 1999, *ASPC*, 163, 283  
Pahre M.A., Djorgovski S.G., de Carvalho R.R., 1998, *ApJ*, 116, 1591  
Robertson B., Cox T.J., Hernquist L., Franx M., Hopkins P.F., Martini P., Springel V., 2006, *ApJ*, 641, 21  
Sandage A., Perelmuter J., 1990, *ApJ*, 361, 1  
Sandage A., Visvanathan N., 1978a, *ApJ*, 223, 707  
Sandage A., Visvanathan N., 1978b, *ApJ*, 225, 742  
Schade D., Barrientos L.F., López-Cruz O., 1997, *ApJ*, 477, L17  
Sellwood J.A., McGaugh S.S., 2005, *ApJ*, 634, 70  
Springel V., et al., 2005, *Nature*, 435, 629  
Treu T., Ellis R.S., Liao T.X., van Dokkum P.G., Tozzi P., Coil A., Newman J., Cooper M., Davis M., 2005, *ApJ*, 633, 174  
Trujillo I., Burkert A., Bell E.F., 2004, *ApJL*, 600, L39  
Tully R.B., Fisher J.R., 1977, *A&A*, 54, 661  
van der Ven G., van Dokkum P.G., Franx M., 2003, *MNRAS*, 344, 924  
van der Wel A., Franx M., van Dokkum P.G., Huang J., Rix H.-W., Illingworth G. D., 2006, *ApJ*, 636, L21  
van der Wel A., Franx M., van Dokkum P. G., Rix H.-W., Illingworth G. D., Rosati P., 2005, *ApJ*, 631, 145  
van Dokkum P.G., Franx M., Kelson D.D., Illingworth G.D., 2001, *ApJ*, 553, L39  
van Dokkum P.G., Franx M., 1996, *MNRAS*, 281, 985  
Wilman R.J., Gerssen J., Bower R.G., Morris S.L., Bacon R., de Zeeuw P.T., Davies R.L., 2005, *Nature*, 436, 227  
Ziegler B., Thomas D., Böhm A., Bender R., Fritz A., Maraston C., 2005, *A&A*, 433, 519